Supporting Information

Green-/NIR-Light-Controlled Rapid Photochromism Featuring Reversible Thermally Activated Delayed Fluorescence and Photoelectronic Switching

Ziyong Li, Ji-Rui Zhang, Xu-Ke Tian, Shuren Yang, Si Chen, Hui Zhou and Xiao-Gang Yang*

College of Chemistry and Chemical Engineering, College of Food and Drug, Luoyang Normal University, Luoyang, 471934, P. R. China. E-mail: yxg2233@126.com.

1. General information

1.1 Materials

All manipulations were carried out under a nitrogen atmosphere by using standard Schlenk techniques unless otherwise stated. THF and toluene was distilled under nitrogen from sodium-benzophenone. DMF was dried by $MgSO_4$ and distilled under reduced pressure. The intermediates **1**[1], **3**[2], **4**[2] and **5**[3] were prepared by reported literature method, respectively. All other starting materials were obtained commercially as analytical-grade from Energy Chemical Reagent Co., Ltd (Shanghai, China) and used without further purification.

1.2 Instruments

^{1}H and ^{13}C NMR spectra were collected on German BRUKER AVANCE III 400 MHz (all the chemical shifts are relative to TMS). High resolution mass spectra were obtained on SCIEX X-500R QTOF (ESI mode). All the absorption spectra were collected on a SHIMADZU UV-2600 UV-Vis spectrophotometer, and the fluorescence spectra were obtained on a Hitachi Model F-4500 fluorescent spectrophotometer. The photoluminescence (PL) and PL decay curves were determined by a fluorescent spectrophotometer (FLS1000). In the photochromic experiments, the visible light irradiation experiment was carried out using a 30 W Green lamp (530 nm) and 30 W Near infrared lamp (770 nm), respectively. The morphology of all samples were investigated by using a field emission scanning electron microscope (SEM Sigma 500).

Photo-electrochemical measurements were tested in a three-electrode system on CHI 660E electrochemical workstation. The working electrodes were prepared by dropping the chloroform solution of **BFBDTE(o)** and **BFBDTE(c)** on the indium tin oxide (ITO) electrode, respectively. Ag/AgCl and platinum wire was used as reference and counter electrodes, respectively. All the electrochemical measurements were performed in 0.5 M Na_2SO_4 solution.

1.3 Determination of the cyclization and cycloreversion quantum yields

The cyclization and cycloreversion quantum yields of **BFBDTE** were determined according to the standard procedure reported in previous literatures[4,5]. For the cyclization quantum yields, potassium ferrioxalate ($K_3[Fe(C_2O_4)_3]$) was used as actinometer[6]. The light intensity at 520 nm was determined by following steps: i) 3.0 mL of 0.15 M $K_3[Fe(C_2O_4)_3]$ solution in 0.05 M H_2SO_4 was irradiated for 180 s; ii) 0.5 mL phenanthroline (0.1 wt % in 0.5 M H_2SO_4 /1.6 M NaOAc) were added subsequently; iii) measuring the absorpance at 510 nm before and after irradiation. The light intensity could be calculated via Eq. (1).

$$I_0 = \frac{\Delta A_{510nm}}{\Delta t * \varepsilon_{510nm} * \emptyset_{irr} * 1000} * \frac{3.5mL}{3.0mL} \qquad (1)$$

In which ΔA_{510nm} is the difference of the absorption at 510 nm for an irradiated versus a nonirradiated solution, Δt is the irradiation time, ε_{510nm} is 11100 M^{-1} cm^{-1} and Φ_{irr} is the quantum yield at the irradiation wavelength (0.65 for 520 nm).

Because the wavelength of the irradiation light that was needed for the ring-opening was out of the range for ferrioxalate actinometry (220-550 nm). Therefore,

for the cycloreversion quantum yields of **BFBDTE**, aberchrome 670 was used as actinometer[6]. The light intensity at 600 nm was determined by following steps: i) 3.0 mL aberchrome 670 solution (1.0×10^{-4} M in toluene) was irradiated with 365 nm light; ii) the formed isomer was irradiated back with 600 nm light, iii) measuring the absorpance at 519 nm before and after irradiation. The light intensity at 600 nm could be calculated via Eq. (2).

$$I_0 = \frac{\Delta A_{519nm}}{\Delta t * \varepsilon_{519nm} * \emptyset_{irr} * 1000 * (1 - 10^{-A'})} \qquad (2)$$

In which ΔA_{519nm} is the difference of the absorption at 519 nm before and after irradiation, Δt is the irradiation time, ε_{519nm} is 7760 M^{-1} cm^{-1}, Φ_{irr} is the quantum yield at the irradiation wavelength (0.27 for 600 nm), $1\text{-}10^{-A'}$ is the percentage of absorbance photons by the solution at irradiation wavelength, and A' is the initial absorpance at the irradiation wavelength.

Then, the solutions of ring-open isomer **BFBDTE(o)** (3.0 mL, 2.0×10^{-5} M) were irradiated with the same investigated light source, and the changes at corresponding maximum absorption wavelength were measured immediately. The cyclization quantum yields could be calculated via Eq. (3). Moreover, the similar operations were performed on ring-closed isomer **BFBDTE(c)**, and the cycloreversion quantum yields could also be calculated via Eq. (3).

$$\emptyset = \frac{\Delta A / \Delta t}{(1 - 10^{-A'}) * \varepsilon * I_0 * 1000} \qquad (3)$$

In which $\Delta A/\Delta t$ is the change rate of absorbance upon irradiating at excitation

wavelength, $1\text{-}10^{-A'}$ is the percentage of absorbance photons by the solution at irradiation wavelength, A' is the absorbance of open-form at excitation wavelength, ε is extinction coefficient at detection wavelength, and I_0 is the light intensity calculated above.

1.4 Determination of the fluorescence quantum yields

The fluorescence quantum yields (Φ_f) of **BFBDTE(o)** in the various solvents were approximatively determined according to the following equation:

$$\emptyset_s = \emptyset_{ref} \times \frac{F_s}{F_{ref}} \times \frac{A_{ref}}{A_s} \times \frac{n_s^2}{n_{ref}^2}$$

in which Φ_{ref} is the fluorescence quantum yield of reference, F is the area under the emission spectra, A is the absorbance at the excitation wavelength, n is the refractive index of solvent. s and ref stand for sample and reference, respectively. We chose rhodamine 6G in water (Φ_{ref} = 0.75, λ_{ex} = 488 nm) as the reference. Absorbance of the unknown samples and the standard should be similar and small[7].

1.5 Preparation of the PMMA film

The PMMA films were prepared by dissolving **BFBDTE** (5.0 mg) and PMMA (100 mg) in $CHCl_3$ (2 mL), then the uniform solution was coated on the quartz plate (1.0 × 3.0 cm). The PMMA films were dried in air and stored in darkness.

1.6 X-ray single crystal structure

Single-crystal X-ray diffraction data were gathered at room temperature (293 K) on an Oxford Diffraction SuperNova area-detector diffractometer equipped with Mo-Kα

X-ray source (λ = 0.71073 Å). The data reduction was treated by using CrysAlis Pro software[8]. The crystal structure was solved by SHELXS-2014 program[9]. Crystallographic data of **BFBDTE** was listed in Table S1. The CIF file of **BFBDTE** (CCDC No. 2171748) can be gained free of charge via http://www.ccdc.cam.ac.uk/conts/retrieving.html.

1.7 Theoretical calculations.

The density functional theory (DFT) calculations were performed by Material Studio software package Dmol[3] module.[10,11] The structure modes for the **BFBDTE(o)** and **BFBDTE(c)** were optimized by Perdew-Wang (PW91)[12] generalized gradient approximation (GGA) method.

2. Experimental section

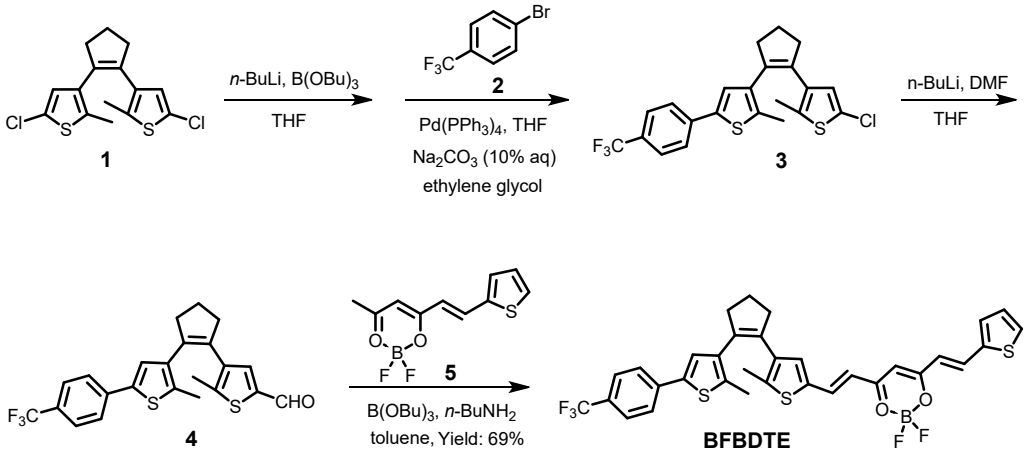

Scheme S1. Synthetic route of **BFBDTE**.

To a solution of intermediate **4** (433 mg, 1.0 mmol) and **5** (242 mg, 1.0 mmol) in toluene (3.0 mL) was added $B(OBu)_3$ (0.41 mL, 1.5 mmol) and *n*-Butylamine (25 μL, 0.25 mmol), and the resulting solution was stirred at 65 °C for 24 h. After cooling to

room temperature, the solution was concentrated under reduced pressure and the residue was purified by column chromatography (silica gel: 200-300, PE : DCM = 1 : 2) to obtain the target **BFBDTE** as an orange solid (Yield: 69%). ^{1}H NMR (400 MHz, $CDCl_3$) δ 8.14 (d, *J* = 15.2 Hz, 1H), 8.03 (d, *J* = 15.0 Hz, 1H), 7.59 (br, 4H), 7.54 (d, *J* = 5.0 Hz, 1H), 7.40 (d, *J* = 3.4 Hz, 1H), 7.14-7.12 (m, 2H), 7.07 (s, 1H), 6.46 (d, *J* = 15.2 Hz, 1H), 6.28 (d, *J* = 15.0 Hz, 1H), 5.94 (s, 1H), 2.87-2.75 (m, 4H), 2.15-2.11 (m, 2H), 2.06 (s, 3H), 1.98 (s, 3H). ^{13}C NMR (100 MHz, $CDCl_3$) δ 179.08, 178.29, 143.46, 139.87, 139.82, 138.94, 138.39, 138.32, 137.49, 136.46, 136.17, 136.04, 135.94, 133.80, 133.60, 131.33, 128.91, 128.57, 125.82, 125.79, 125.22, 124.97, 122.73, 119.32, 117.77, 101.92, 38.44, 38.25, 22.92, 22.80, 15.35, 14.47. HRMS (ESI-TOF) m/z: [M - F] Calcd for $C_{33}H_{26}BF_4O_2S_3$ 637.1124; Found 637.1133; $[M + H]^+$ Calcd for $C_{33}H_{27}BF_5O_2S_3$ 657.1186; Found 657.1196; $[M + NH_4]^+$ Calcd for $C_{33}H_{30}BF_5NO_2S_3$ 674.1452; Found 674.1470; $[M + Na]^+$ Calcd for $C_{33}H_{26}BF_5NaO_2S_3$ 679.1006; Found 679.1010; $[M + K]^+$ Calcd for $C_{33}H_{26}BF_5KO_2S_3$ 695.0745; Found 695.0756.

3. Supporting Figures

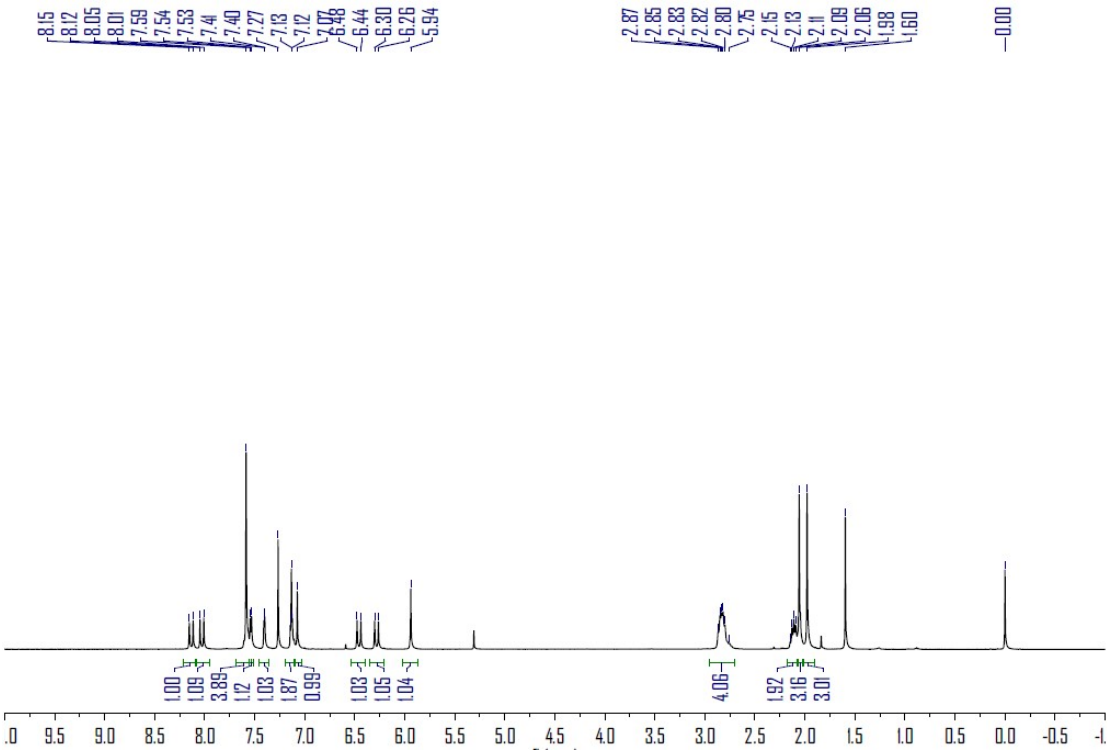

Figure S1. 400 MHz ^{1}H NMR spectrum of **BFBDTE** in $CDCl_3$ at room temperature.

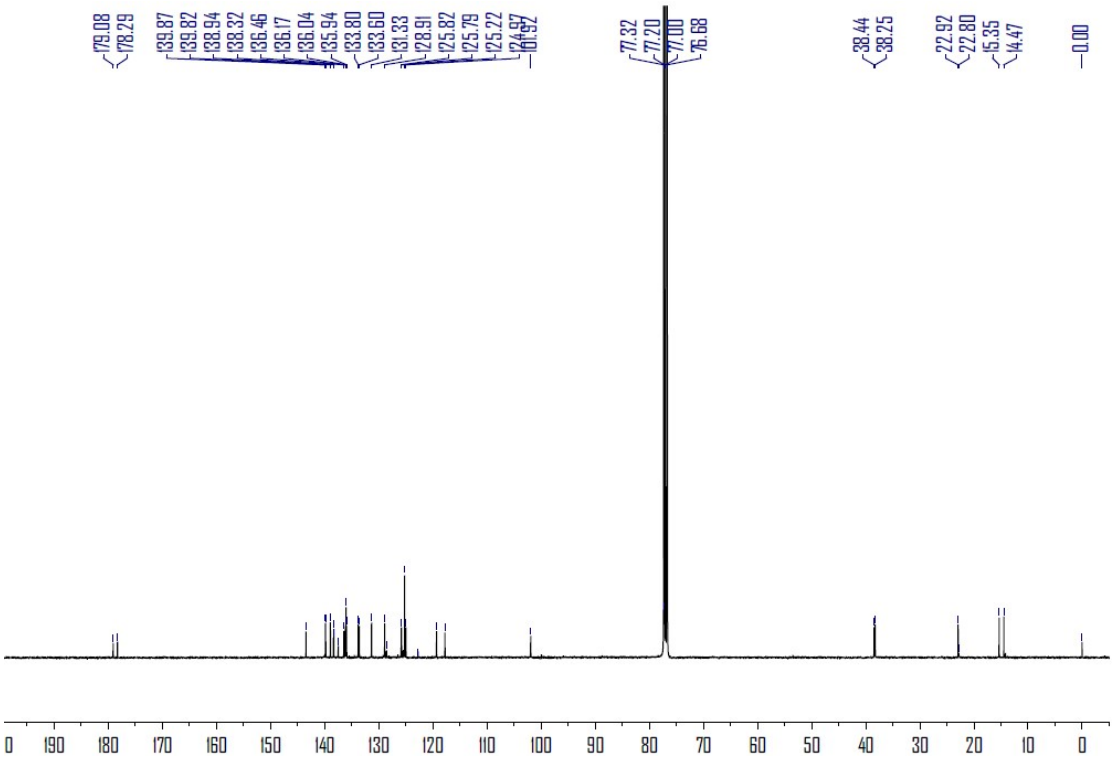

Figure S2. 100 MHz ^{13}C NMR spectrum of **BFBDTE** in $CDCl_3$ at room temperature.

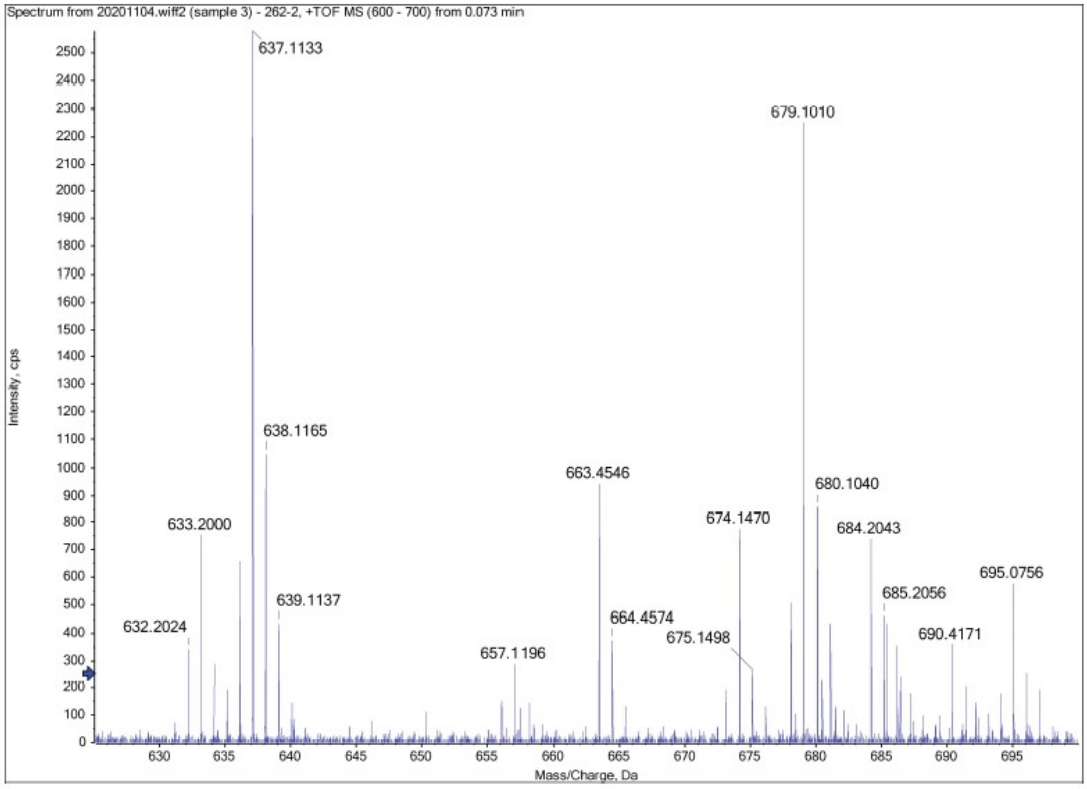

Figure S3. HRMS of **BFBDTE**.

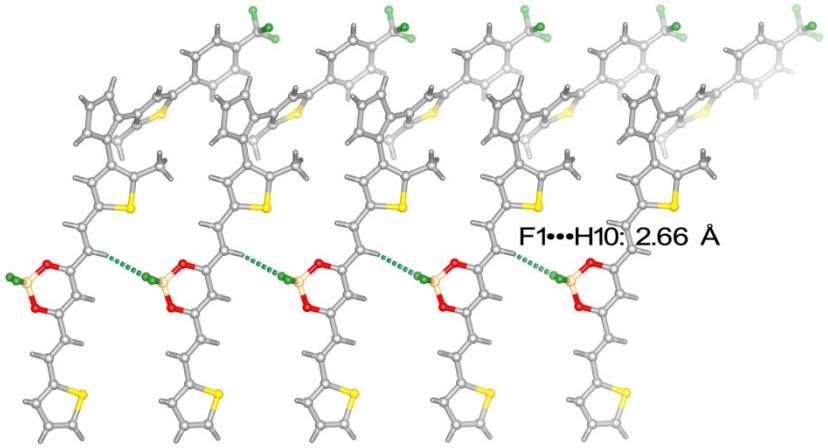

(a)

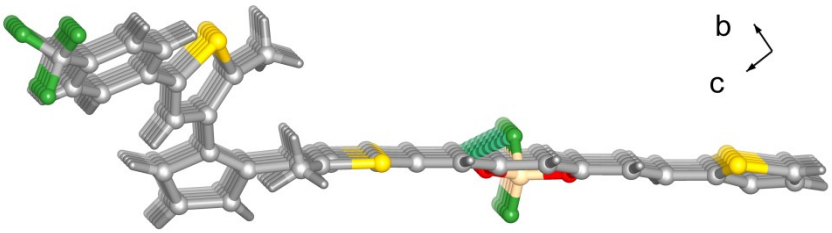

(b)

Figure S4. View of the 1D chain of **BFBDTE** along c (a) and a (b) direction extended by C-H···F hydrogen bonding.

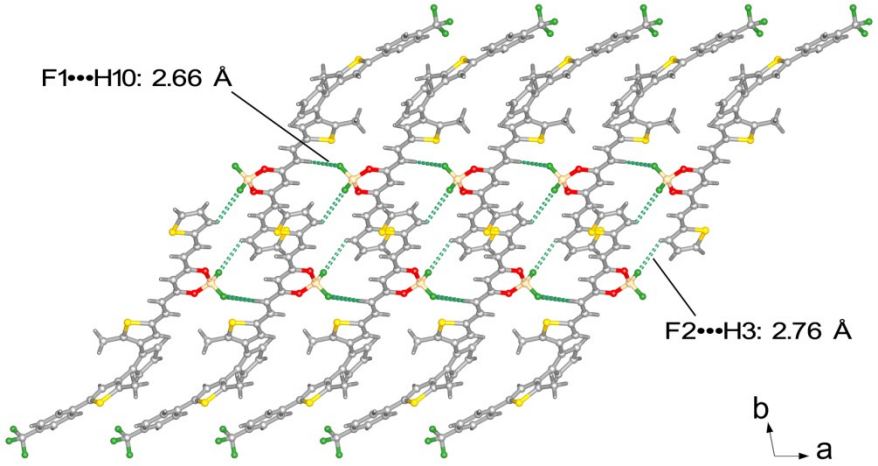

(a)

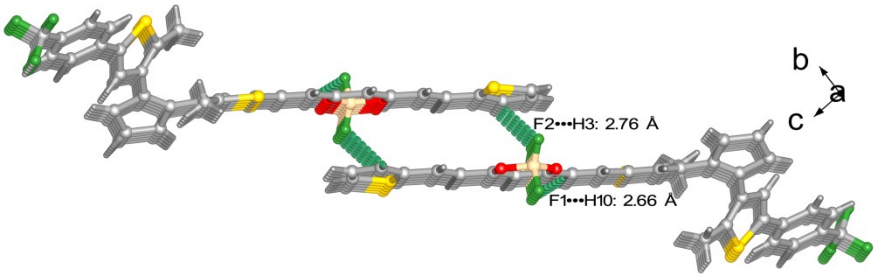

(b)

Figure S5. View of the 1D double-strand chain of **BFBDTE** along c (a) and a (b) direction extended by C-H···F hydrogen bonding.

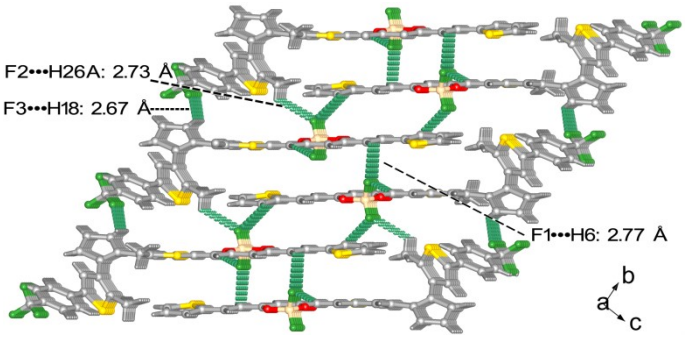

(a)

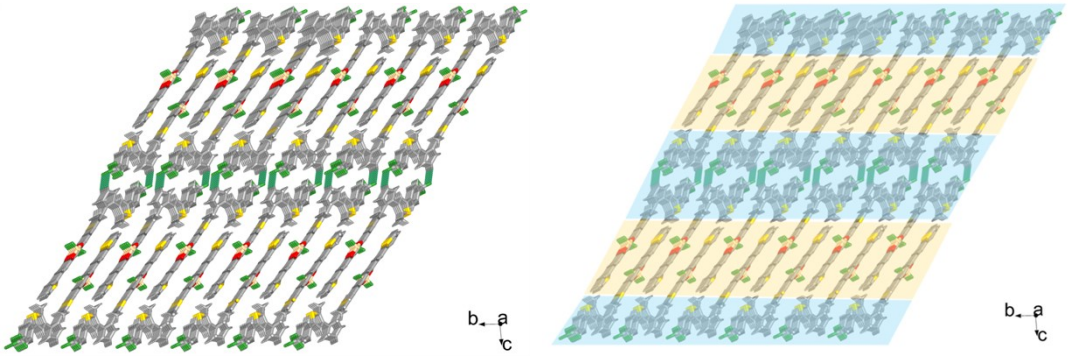

(b)

Figure S6. (a) View of the 2D layer structure of **BFBDTE** extended by C–H···F hydrogen bonding. (b) View of the 3D structure of **BFBDTE** along a direction extended by C-H···F hydrogen bonding between adjacent 2D layers showing alternant arrangement of BF_2bdk electron acceptor (yellow region) and DTE electron donor (pale blue region).

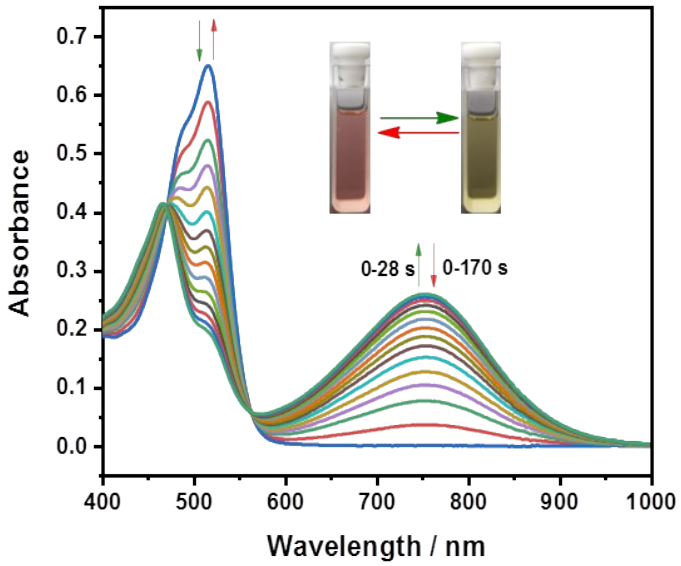

Figure S7. The absorption spectra changes of **BFBDTE** in $CHCl_3$ (2.0×10^{-5} mol/L) upon alternating irradiation with green light at 520-530 nm and NIR light at 760-770 nm. Inset: corresponding color changes upon photoirradiation.

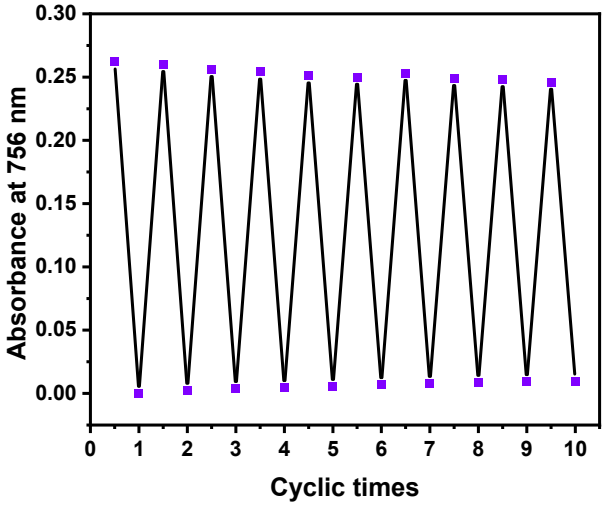

Figure S8. Fatigue resistance of **BFBDTE** in $CHCl_3$ (2.0×10^{-5} mol/L) upon alternating irradiation with green light at 520-530 nm and NIR light at 760-770 nm over ten cycles.

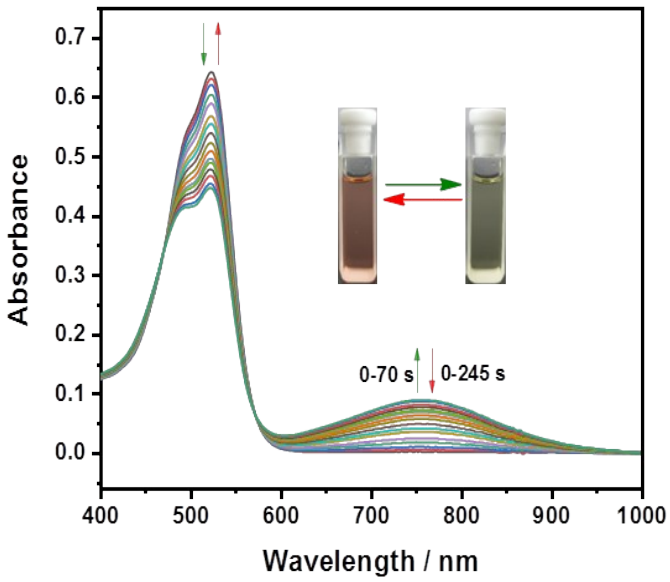

Figure S9. The absorption spectra changes of **BFBDTE** in DMSO (2.0×10^{-5} mol/L) upon alternating irradiation with green light at 520-530 nm and NIR light at 760-770 nm. Inset: corresponding color changes upon photoirradiation.

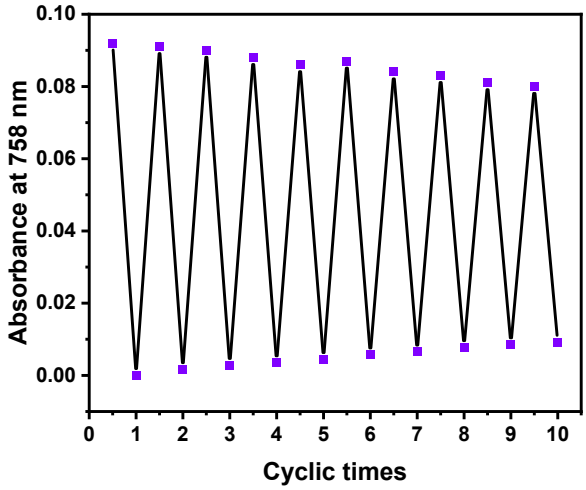

Figure S10. Fatigue resistance of **BFBDTE** in DMSO (2.0×10^{-5} mol/L) upon alternating irradiation with green light at 520-530 nm and NIR light at 760-770 nm over ten cycles. The degradation of photoreaction performance for **BFBDTE** can be assigned to the large polarity and viscosity of DMSO, which would hinder the photochromic reaction. Meanwhile, the weak oxidation of DMSO would promote the degradation of BFBDTE.

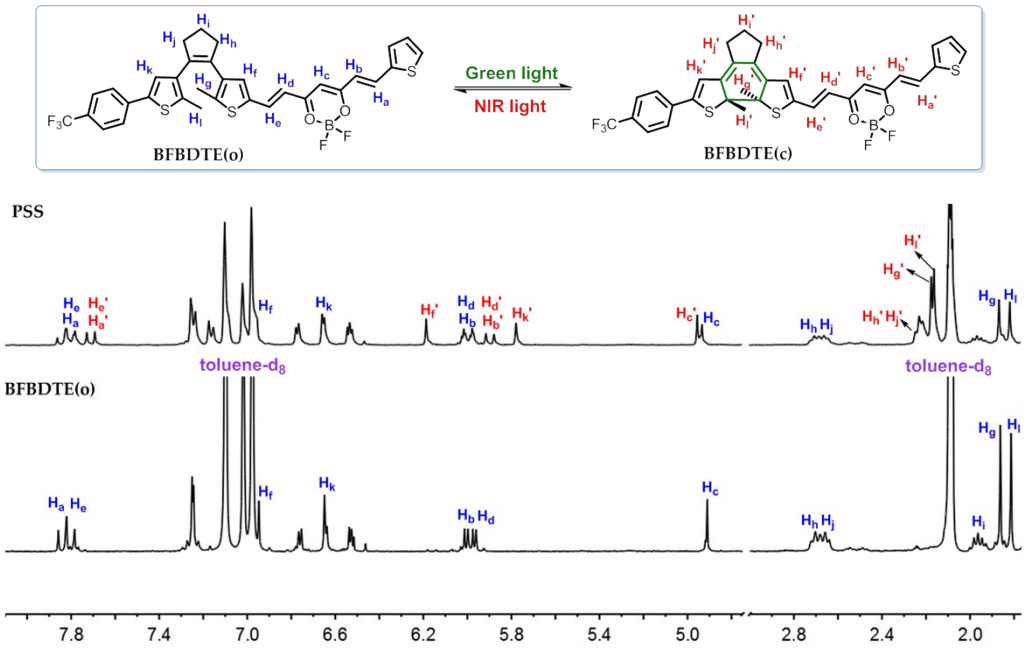

Figure S11. Partial ^{1}H NMR spectral variations of **BFBDTE** upon irradiation with green light in toluene-d_8.

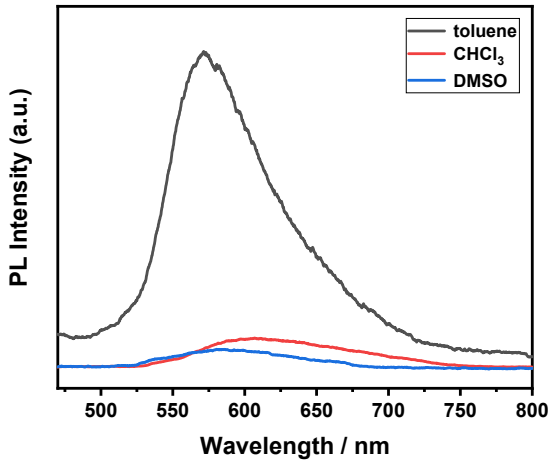

(a)

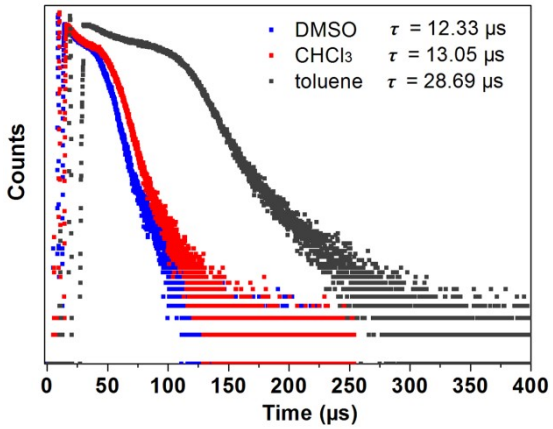

(b)

Figure S12. PL spectra (a) and (b) decay curves of **BFBDTE** under delayed mode at room temperature in different solvents (λ_{ex} = 450 nm).

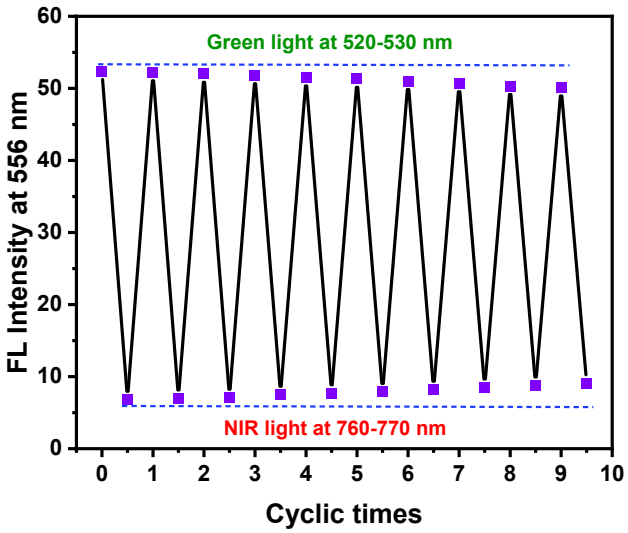

Figure S13. Fluorescence fatigue resistance of **BFBDTE** for ten cycles in toluene.

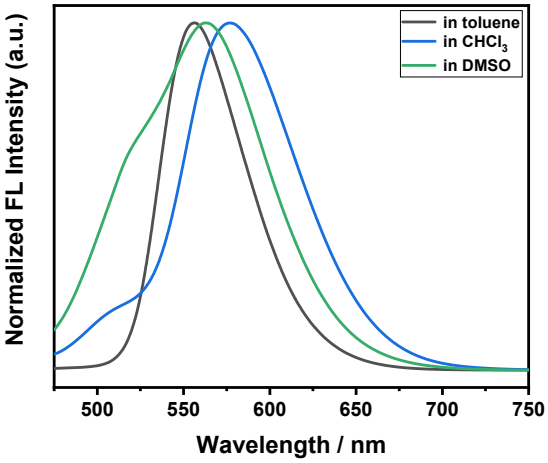

Figure S14. The prompt fluorescence spectra of **BFBDTE** in different solvents (2.0×10^{-5} mol/L) before irradiation.

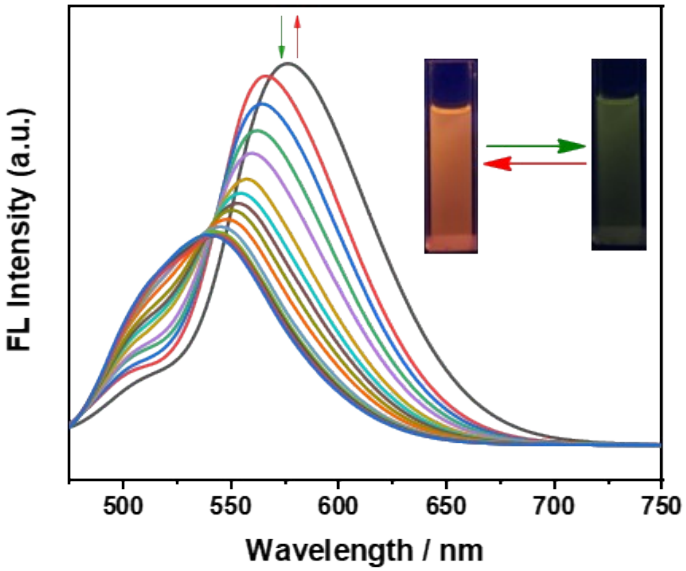

Figure S15. The prompt fluorescence spectra changes of **BFBDTE** in $CHCl_3$ (2.0×10^{-5} mol/L) upon alternating irradiation with green and NIR light. Inset: corresponding fluorescence changes upon photoirradiation.

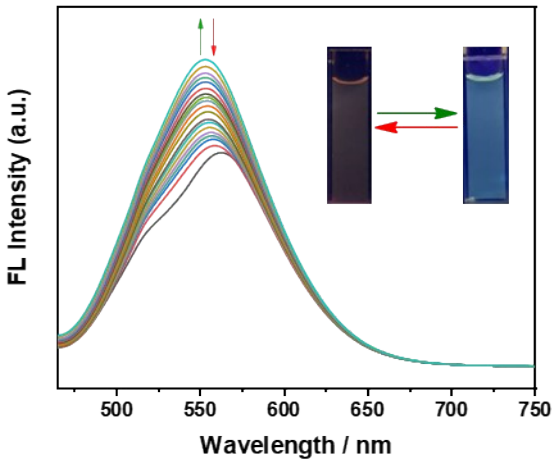

Figure S16. The prompt fluorescence spectra changes of **BFBDTE** in DMSO (2.0×10^{-5} mol/L) upon alternating irradiation with green and NIR light. Inset: corresponding fluorescence changes upon photoirradiation.

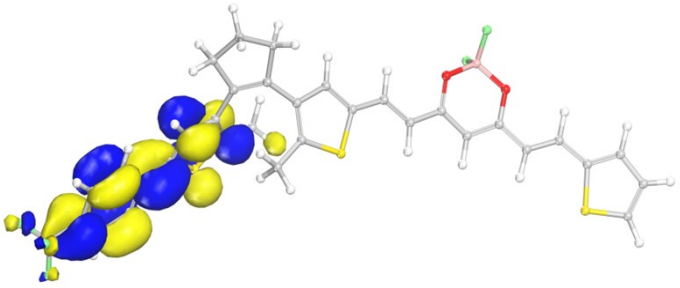

(a)

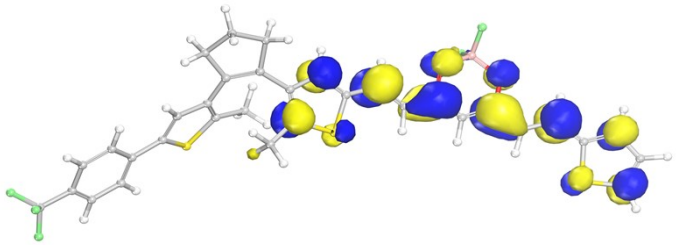

(b)

Figure S17. View of HOMO (a) and LUMO (b) for the profiles based on DFT calculations of **BFBDTE(o)**.

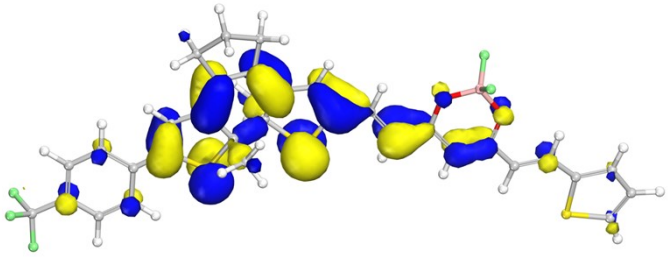

(a)

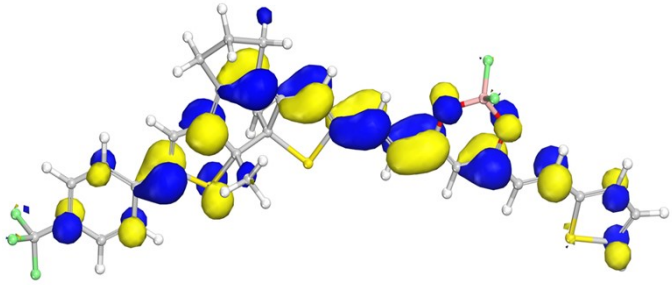

(b)

Figure S18. View of HOMO (a) and LUMO (b) for the profiles based on DFT calculations of **BFBDTE(c)**.

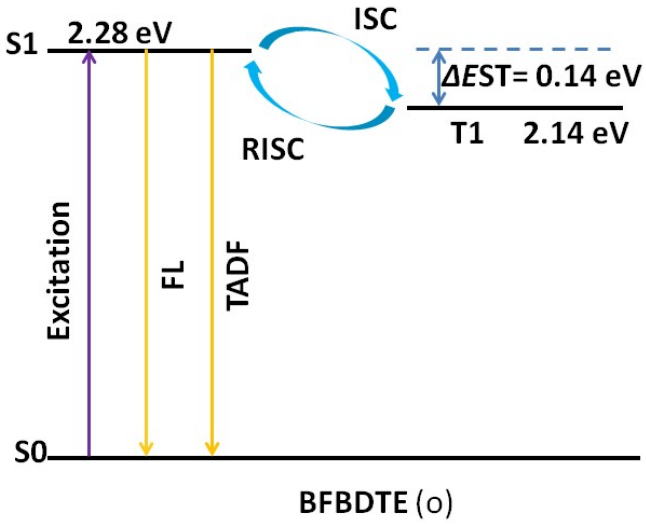

Figure S19. Schematic illustration of the photophysical process for the cycloreversion state of **BFBDTE(o)**.

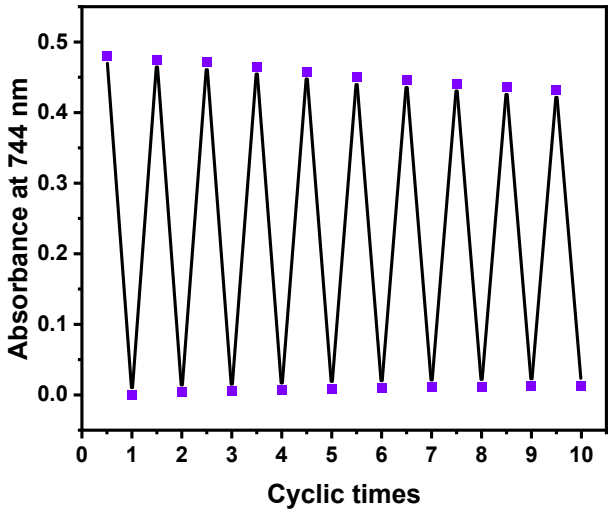

Figure S20. The fatigue resistance of **BFBDTE** for ten cycles in the PMMA film.

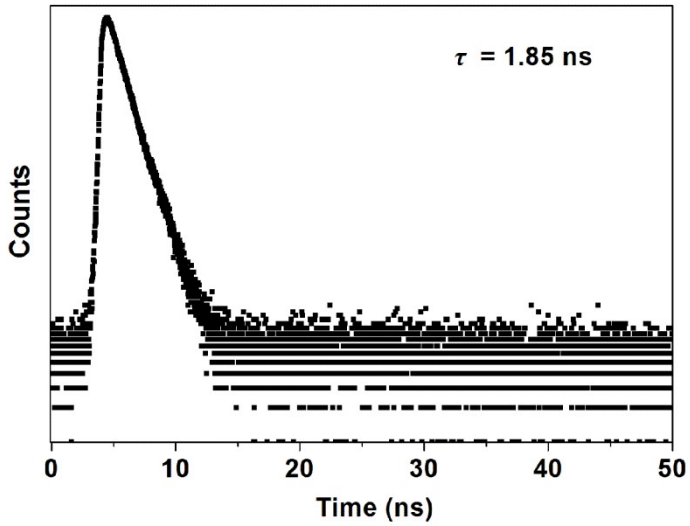

(a)

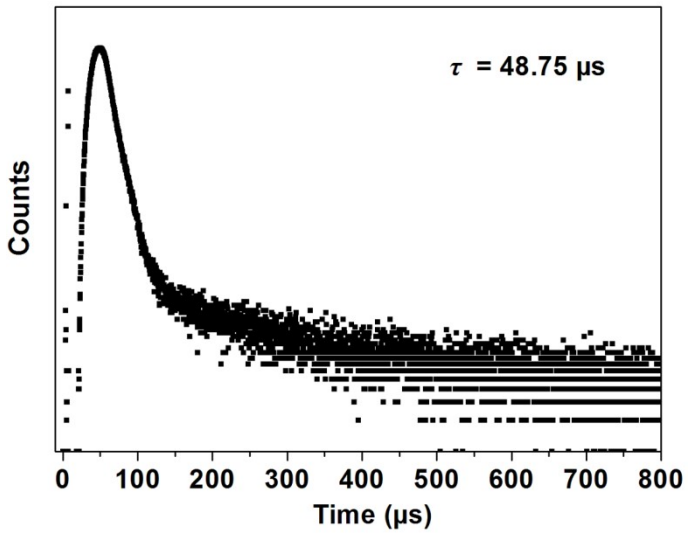

(b)

Figure S21. Prompt (a) and delayed (b) fluorescence decay curves of **BFBDTE(o)** doped in PMMA film.

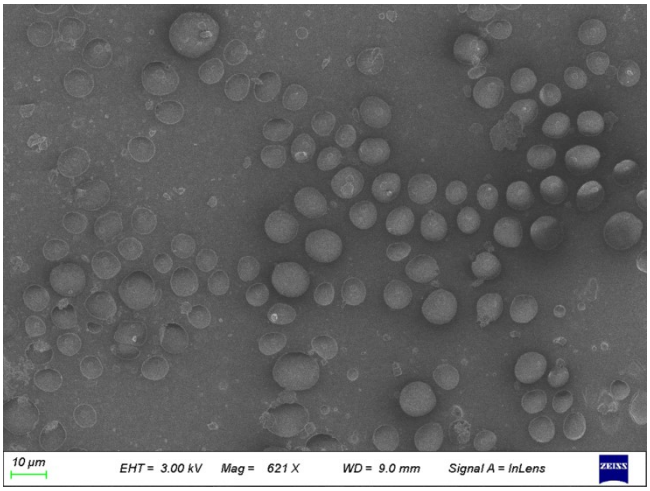

(a)

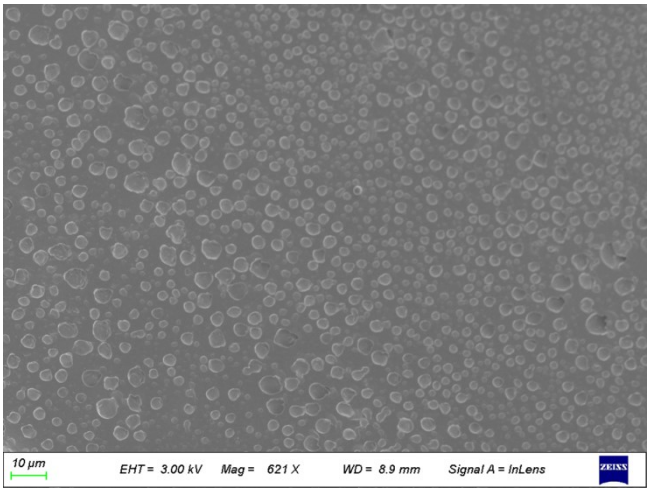

(b)

Figure S22. SEM images of **BFBDTE(o)** (a) and **BFBDTE(c)** (b) chloroform solution dropped and dried on the indium tin oxide (ITO) substrat.

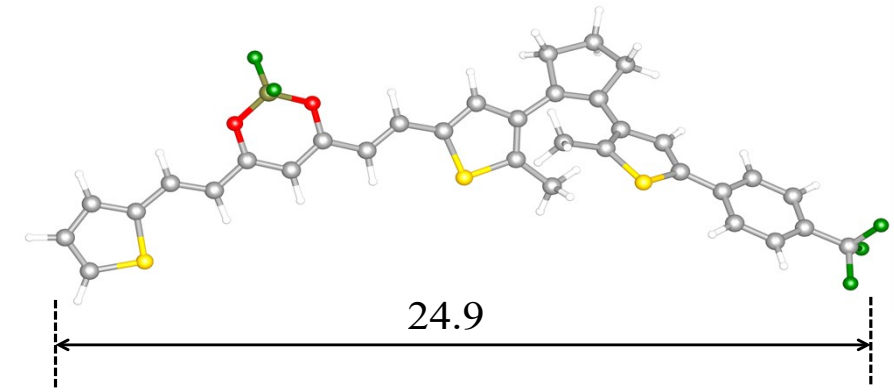

(a)

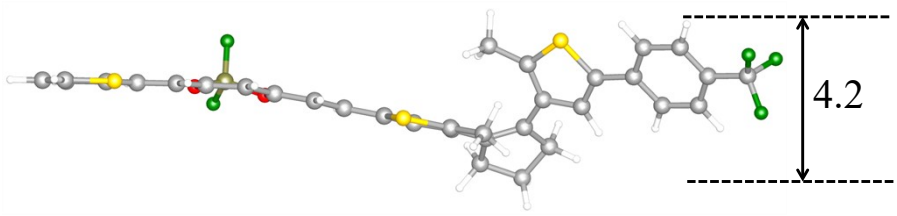

(b)

Figure S23. Front (a) and side view (b) of **BFBDTE(o)** based on DFT calculations.

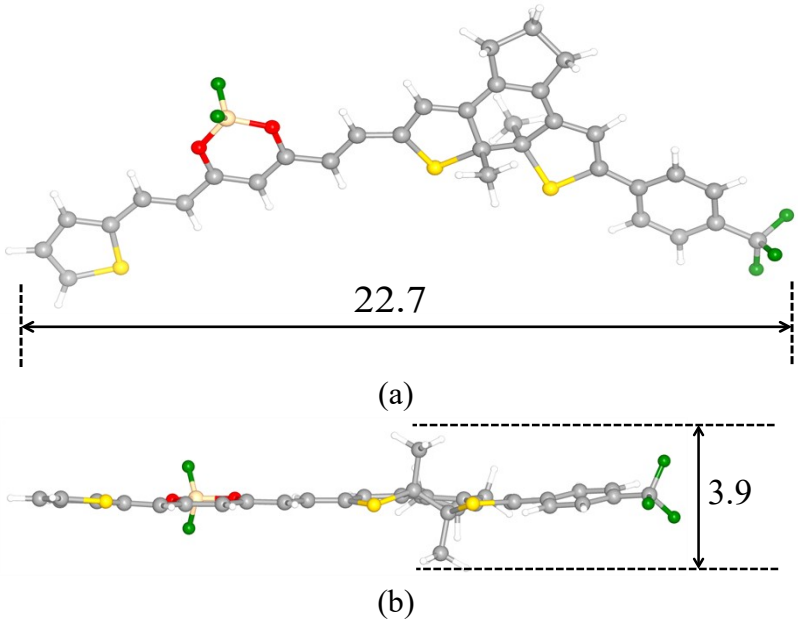

Figure S24. Front (a) and side view (b) of **BFBDTE(c)** based on DFT calculations.

4. Supporting Tables

Table S1. Crystallographic data for **BFBDTE**.

Compound	**BFBDTE**
Empirical formula	$C_{33}H_{23}BF_5O_2S_3$
Formula weight	653.50
Crystal system	triclinic
Space group	$P\bar{1}$
a (Å)	7.3149(12)
b (Å)	8.4664(13)
c (Å)	25.630(4)
α (°)	93.482(13)
β (°)	94.312(13)
γ (°)	100.726(14)
V (Å^3)	1550.6(4)
Z	2
D (g cm^{-3})	1.400
μ (mm^{-1})	0.299
R_{int}	0.1135
Goof	1.004
R_1 ($I>2\sigma(I)$)	0.1095
wR_2 ($I>2\sigma(I)$)	0.1875

Table S2. Photochromic parameters of **BFBDTE** in various organic solvents (2.0×10^{-5} M) and the PMMA film.

Solvents	**λ_{max}[a] (nm) ($\varepsilon\times10^{-4}$, M^{-1} cm^{-1})**	**λ_{max}[b] (nm) ($\varepsilon\times10^{-4}$, M^{-1} cm^{-1})**	**$\varphi_{o\text{-}c}$[c]**	**$\varphi_{c\text{-}o}$[d]**
toluene	478 (3.12) 509 (3.68)	727 (1.88)	0.56	0.031
$CHCl_3$	516 (3.26)	756 (1.31)	0.24	0.026
DMSO	523 (3.22)	758 (0.46)	0.08	0.006
PMMA	482 (7.01) 510 (7.05)	744 (2.40)	--	--

[a]Absorption maxima of ring-open isomers; [b]absorption maxima of ring-closed isomers; [c]cyclization quantum yields; [d]cycloreversion quantum yields, respectively.

Table S3. The photophysical data of **BFBDTE** in various organic solvents (2.0×10^{-5} mol/L) and the PMMA film.

Solvents	$\lambda_{em}{}^{a}$ **(nm)**	$\tau_{PF\ (ns)}{}^{b}$	$\tau_{DF\ (\mu s)}{}^{c}$	$\Phi_f{}^{d}$ **(%)**
toluene	556	1.73	28.57	24
$CHCl_3$	577	1.26	12.2	10
DMSO	564	1.04	9.71	1.3
PMMA	569	1.85	48.75	15

[a]Fluorescence emission maxima; [b]the prompt fluorescence lifetime; [c]the TADF lifetime; [d]fluorescence quantum yield determined by a standard method with rhodamine 6G in water ($\Phi_f = 0.75$, $\lambda_{ex} = 488$ nm) as reference before irradiation with green light.

5. Supporting References

(1) L. N. Lucas, J. J. D. Jong, J. H. Esch, R. M. Kellogg, B. L. Feringa, *Eur. J. Org. Chem.,* 2003, **2003**, 155.

(2) Z. Li, M. Li, G. Liu, Y. Wang, G. Kang, C. Li, H. Guo, *Dyes Pigments,* 2019, **160**, 597.

(3) Z. Li, Y. Dai, Z. Lu, Y. Pei, H. Chen, L. Zhang, Y. Duan, H. Guo, *Chem. Commun.,* 2019, **55**, 13430.

(4) S. Fredrich, R. Göstl, M. Herder, L. Grubert, S. Hecht, *Angew. Chem. Int. Ed.,* 2016, **55**, 1208.

(5) H. Xi, Z. Zhang, W. Zhang, M. Li, C. Lian, Q. Luo, H. Tian, W. -H. Zhu, *J. Am. Chem. Soc.,* 2019, **141**, 18467.

(6) M. Montalti, A. Credi, L. Prodi, M. T. Gandolfi, Handbook of Photochemistry, 3rd ed.; CRC Press: Boca Raton, 2006.

(7) A. P. Glaze, H. G. Heller, J. Whittall, *J. Chem. Soc. Perk. Trans.,* 1992, **2**, 591.

(8) CrysAlisPro, Rigaku Oxford Diffraction, Version 1.171.39.6a.

(9) G. M. Sheldrick, *Acta Crystallogr. Sect. A,* 2008, **64**, 112.

(10) *a*) B. Delley, *J. Chem. Phys*. 1990, *92*, 508; *b*) B. Delley, *J. Chem. Phys*., 2000, **113**, 7756.

(11) Dmol^3 Module, MS Modeling, Version 2.2; Accelrys Inc.: San, Diego, 2003.

(12) J. P. Perdew, J. A. Chevary, S. H. Vosko, K. A. Jackson, M. R. Pederson, D. J. Singh and C. Fiolhais, *Phys. Rev. B,* 1992, **46**, 6671.